Jestr

Journal of Engineering Science and Technology Review 17 (1) (2024) 122 - 130

Research Article

JOURNAL OF
Engineering Science and Technology Review

www.jestr.org

Simulation and Evaluation of GAN-based Implementation of Infrared Texture Generation

Yunyun Wu[1,2,3], Han Liu[1,2], Xia Kong[1,3,*], Min Deng[1,3] and Youfeng Li[1,3]

[1]*School of Computer and Information Science, Hubei Engineering University, Xiaogan Hubei 432000, China*
[2]*School of Artificial Intelligence, Hubei University, Wuhan Hubei, 430062, China*
[3]*Institute for AI Industrial Technology Research, Hubei Engineering University, Xiaogan Hubei, 432000, China*

Received 21 October 2023; Accepted 13 January 2024

Abstract

At present, the demand for the simulation technology of infrared view is markedly expanding. However, the related main research orientations are influenced by numerous factors. Thus, the availability of infrared images for special scenes is difficult to determine, and their practical applications are limited. This study proposed a method based on generative adversarial network (GAN) to reveal its influence on the generation of infrared texture and produce infrared texture in infrared view simulation. By combining the needs of texture generation in infrared simulation and the superiority of image style transfer in texture generation, three algorithms for style transfer based on GAN, namely, Algorithms I, II, and III, were introduced to establish pretrained models. Simulation results of the three models were then evaluated using histograms, structural similarity (SSIM), and peak signal-to-noise ratio (PSNR), and the effects of colors of the infrared images in the texture generation were compared. The validity of these models was also verified. Results demonstrate that infrared images in a specified scene can be simulated without the need for a large number of training datasets, and the simulation images generated by transferring in black-and-white infrared style images are better than those in color infrared style images. The histogram evaluation index shows that Algorithm III is higher than Algorithms I and II by approximately 0.06. The SSIM evaluation index reveals that Algorithm II is higher than Algorithms I and II by 0.09 and 0.06 dB, respectively. The PSNR evaluation index indicates that Algorithm III is higher than Algorithms I and II by approximately 0.31 dB. Thus, this study provides a practical value in the field of infrared simulation technology.

Keywords: Artificial intelligence, Image Style Transfer, Generative adversarial network, Infrared texture generation

1. Introduction

The simulation technology of infrared view generates infrared scene images through computer simulation, which can vividly show infrared images of targets and backgrounds under various complex environments or interferences. Thus, this technology provides environments and data for product testing, the design of optoelectronic imaging systems, and the related scene analysis, shortening the development cycle of related products and saving experimental costs. The simulation technology has attracted attention from various countries [1]. Currently, an important research direction of infrared view simulation lies in the generation of images with infrared texture using visible light images. Before the neural network, generating infrared texture according to visible light images mainly involved material classification, image segmentation, and infrared radiation calculation using artificial establishment of mathematical or statistical models.

The demand for infrared view simulation is currently expanding, and the fusion of infrared images with visible light images has become a research hotspot with the increasing demand for target detection and identification as well as military surveillance [2]. A large number of infrared images under special conditions are urgently necessary to be used as research or test objects, but the available resources for such software and technology are limited. Moreover, directly obtaining the relevant infrared images is difficult and costly because the outfield acquisition method can only obtain infrared images under the specific conditions at that time, thus failing to address the needs of numerous experiments on special conditions.

Therefore, scholars have conducted numerous studies on the fusion method of infrared and visible light to increase its convenience for acquiring infrared images under special conditions [3-5]. However, these studies only focused on the fusion of visible light infrared images with the same scene. Other problems, such as high cost of infrared simulation, high technical thresholds, and restricted special scenes, are observed. Therefore, infrared view simulation with low cost and universality is an urgent problem to be solved.

This study focuses on the texture generation in 3D infrared view simulation and introduces image style transfer algorithms from the field of artificial intelligence based on the above analysis. This approach can simulate infrared images under specific conditions, solving the problem of inconvenient acquisition of infrared images under special conditions. Thus, this simulation provides convenience for the research and development of infrared view simulation and has important engineering practical value.

2. State of the art

The software for infrared view simulation with additional functions, superior real-time performance, and strong sense of reality has been successively developed. In recent years, the infrared simulation software exported to China mainly

*E-mail address: wuyunyun_1985@163.com
ISSN: 1791-2377
doi:10.25103/jestr.171.16

include the SE-WORKBENCH [6], a multi-sensor battlefield modeling workbench from France, which can be used to create complex and realistic battlefield environments and simulate the working effects of various sensors. However, the software demands complex operations and high costs. Lepage [7] et al. introduced a method that produces dynamic and realistic infrared scenes. Their method involved complex modeling and simulation processes, possessing high usage complexity and learning costs. Guissin [8] developed the infrared imaging simulator IRISIM, which could simulate the imaging process of wide bandwidth and multispectral infrared imaging systems. However, the simulator required specific hardware and software support, which would increase the operating costs and technical thresholds. VIRSuite [9], which was developed in Australia, was a comprehensive modeling and simulation tool for infrared imaging system aimed at addressing various issues in the design and development process of infrared systems. The tool also had high technical thresholds and requirements for computer hardware. Sakoglu [10] et al simulated mid-wave infrared images with hexagonal array of sampled pixels, which effectively corrected the nonuniformity of infrared images; however, the adaptability to complex scenes and multiple detector types must be improved. Ogata [11] et al. proposed a low-resolution thermal sensor aimed at protecting the privacy of the subject's input in the infrared spectrum by capturing visual information. However, the sensor could be easily influenced by environmental factors, and its monitoring range was limited. Duris [12] et al. fabricated a Ge/ZnS multilayer optical filter for mid-infrared applications, but the filter was sensitive to temperature variations. Mal [13] et al. designed InAsBi PIN photodetector for long wavelength infrared applications. In their design, the detector must be employed within a certain temperature range to ensure performance stability, and the cost was relatively high. Klaassen [14] et al. designed a mid-infrared instrument simulator (MIRISIM) to simulate the on-orbit performance of MIRI imager and spectrometers, but the simulator could only be observed within a specific infrared wavelength range. These techniques were mainly classified in accordance with temperature and radiation prediction models, which were susceptible to environmental factors and with high technical thresholds and costs, increasing the difficulty of its universality.

Scholars in China from universities and research institutes are also conducting numerous works in infrared view simulation, and two mainstream methods are as follows: one is based on the statistical models of random field, and the other is based on multispectral analysis. Shao [15] proposed the infrared texture image generation method based on Markov random field (MRF), generalized long-correlation (GLC), and nonparametric random field models for the first time, which effectively simulated the infrared texture image of relevant scenes. However, using the method in parameter adjustment was complicated, and the data requirements were high. Zhao [16] simulated the infrared texture changes in the related scenery within the daily cycle using visible light texture, but the desired effect for specific types of textures could not be acquired. Gao [17] developed a method to form infrared texture images with temperature fluctuation by considering the effect of altitude and absorptivity on the mean temperature of the materials. However, this method required professional knowledge and skills. Self-developed infrared software systems were also available. Jiang [18] designed an infrared real-time system for simulation of scenarios by analyzing the optoelectronic interference coupling. However, the complexity of the system is high, failing to simulate special scenarios. Zhang [19] et al. introduced a new simulation method for large dynamic infrared scene based on the technology of photonic crystals, which was of strong sense of reality. However, high thresholds and costs were required for the realization and application of the method, and the simulation of complex scenes was also limited. Li [20] et al. built the full-link mathematical model for infrared imaging based on radiation transfer theory, which was easy to implement. The architecture of the proposed system had strong scalability, and generated infrared simulation images were in accordance with the physical laws. However, the simulation framework required high technical thresholds and had certain limitations for simulating infrared imaging in different scenes. Liu [21] constructed a GPU-based infrared simulation system framework by combining OpenGL and OpenGL shading language (GLSL). The system again displayed a high threshold, and limitations were observed for infrared simulation of different scenes. Zhao [22] et al. established a real-time simulation system for the confrontation process of airborne infrared jamming bombs by comprehensively utilizing the Unity3D engine, geographic information system, and computer simulation technology, which also suffered from specific scenario limitations and high technical thresholds.

The above studies mainly used physical modeling methods for infrared view simulation, which were subject to a variety of factors such as temperature and scene and other factors with high the technical thresholds and economic costs. Artificial intelligence methods have been considered in infrared view simulation research to overcome the above deficiency. Gatys et al. [23,24] proposed the GAN-based image style transfer algorithm in 2015. The algorithm emphasized that textures can be described using statistical models of local image features, and the image style transfer algorithm can transfer the style of famous paintings created by art masters to ordinary images. This study investigates the GAN-based image style transfer algorithm for infrared view simulation and proposes three algorithms with different characteristics to simulate the generation of infrared texture using visible/infrared images captured in real time. The characteristics of the different algorithms in the infrared texture generation should be evaluated from multiple perspectives, providing technical supports for infrared view simulation.

The remainder of this study is organized as follows. Section 3 describes the experimental process of the proposed infrared simulation methods and the construction of network models of the infrared image style transfer algorithm. This section also shows the results of the simulation tests as well as the evaluation indexes of the simulation results. Section 4 evaluates the simulation effects of data generated by different algorithms through the prevalent evaluation indexes and finally analyzes the effect of infrared image style transfer algorithms in infrared texture generation. Section 5 summarizes the conclusions.

3. Methodology

The flowchart of the simulation experiment is shown in Fig. 1. After conducting the demand analysis of the infrared view simulation, three algorithms of GAN-based infrared image style transfer are constructed to generate the infrared texture images from visible images. The three algorithms are then evaluated and compared in combination with the actual captured visible-infrared image pairs.

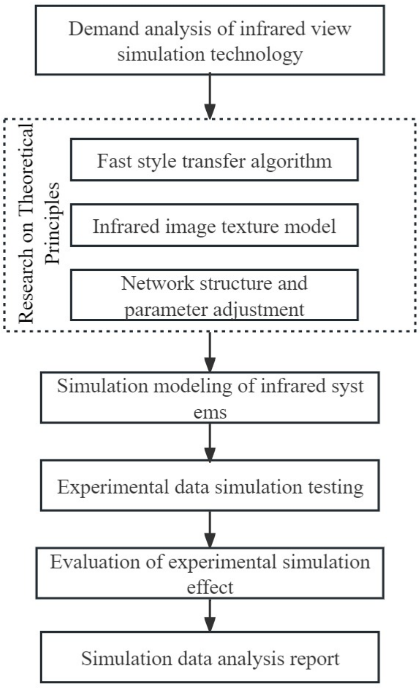

Fig. 1. Flowchat of the research methodlogy

3.1 Model construction of the networks for infrared image style transfer algorithm

The network construction for the infrared image style migration algorithm is based on the visual geometry group network (VGGNet), a deep convolutional network jointly developed by the Computer Vision Group at the University of Oxford and DeepMind. The shallow convolutional layers of the VGGNet are employed to extract low-dimensional and specific information-preserving features such as texture and color; deep convolution layers extract high-dimensional and abstract information such as the shape and location of objects [25]. The actual operation extracts the features of the content images, the style images, and the generated images by VGGNet without fully connected layers, and the generated images are originally initialized as white noise maps. As shown in Fig. 2, the content loss is calculated with content and generated graph features, and the style loss is calculated with style and generated graph features. The two kinds of losses are combined as the total loss. The overall loss is then employed to calculate the gradient of the generated images and then update the generated images.

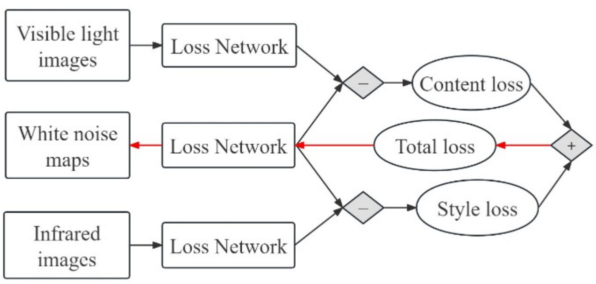

Fig. 2. Block diagram of the principle of infrared image style transfer algorithm

The three algorithms are consistent in their transfer assessment objects and all use the same data pairs to facilitate comparative analysis of the results. The experimental photo pairs for comparison are obtained using a handheld thermal imaging camera, Hikvision HM-TPK20-3AQF/W with a size of 640 × 480. A total of 25 pairs of colored and black-and-white infrared photos are taken, each comprising two photos of the same scene (one of visible light content and one of infrared style of the same scene). The two sets of photo pairs in Fig. 3 are chosen in this study as an example of style transfer. Notably, during the transfer training, the visible light images are selected as the "content maps," the infrared images of different scenes from the visible images are selected as the "style maps," and the images generated by the algorithm are selected as the "effect maps." The "effect maps" generated by transfer in different scenes are evaluated in comparison with the style maps of the same scene in visible light.

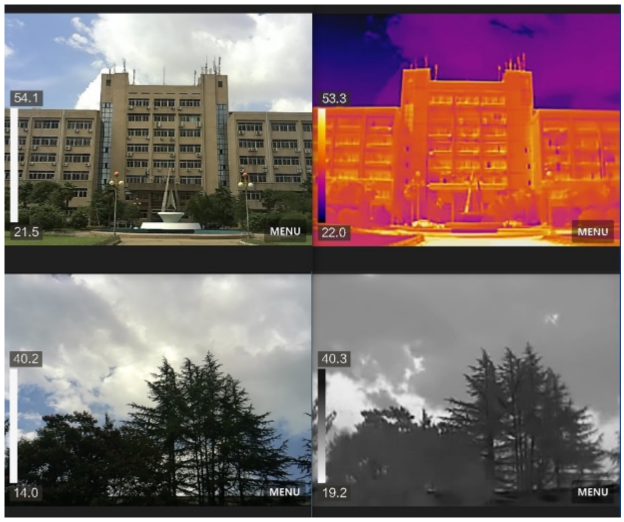

Fig. 3. Examples of visible-infrared image pairs

3.2 Experimental simulation test

A trained model learns a method of extracting the image features. Theoretically, the trained model can also directly extract features from other images, which is the basis of transfer learning. However, this approach is often not as effective as the model retrained on new data but can save training time and is substantially helpful in specific situations. Pretrained network models are employed in the experiment due to limited hardware equipment. The number of iterations for all of these models is set to 1000 to compare the transfer effects of the three algorithms. The prevalent deep learning frameworks are TensorFlow, PyTorch, Keras, MXNet, and Caffe. Among these frameworks, TensorFlow has the advantages of Python interface, scalability, and official support. This study uses TensorFlow based Python environment to build the neural network models.

3.2.1 Algorithm I

Algorithm I is based on the VGG19, in which the model enhances the network depth while ensuring that it has the same perceptual field, which improves the effectiveness of the neural network [26]. Five convolution layers of the original network are used for the extraction of content feature, and different subsets of convolution layers are employed for the style feature extraction. The ratio of content to style weights is 1:100, the fully connected layers are discarded, and the maximum pooling is used. The transfer results are shown in Figs. 4 and 5 (from left to right), which reveal content, style, and effect maps.

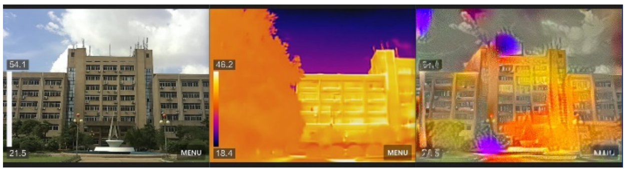

Fig. 4. Comparison of colored infrared style transfer for Algorithm I

Fig. 5. Comparison of black-and-white infrared style transfer for Algorithm I

The two groups of transfer results in Fig. 4 reveal that the effect of the colored map transferred from the infrared style image is visually worse and significantly lost content details. An uneven distribution of colors and image distortion are also observed, but the style characteristics are evident. Fig. 5 shows that the map transferred from the black-and-white infrared style and content details remained intact, but the same style features appear distorted. Overall, the black-and-white infrared style transfer effect is better than that of the colored infrared style.

3.2.2 Algorithm II

Certain modifications are made in the VGG19 model in Algorithm II. The conv5_2 and conv4_2 layers of the network are retained for content feature extraction, and the layers conv1_1, conv2_1, conv3_1, conv4_1, and conv5_1 are employed for the extraction of style features. The fully connected layer is then discarded. In addition, a noise image is given to the input layer at the beginning and iteratively optimized in accordance with the loss function with the increase in training times. The image has the style of a style image and the content of a content image after reaching a certain number of times. The ratio of content to style weights is 1:500. Figs. 6 and 7 show the transfer results of Algorithm II.

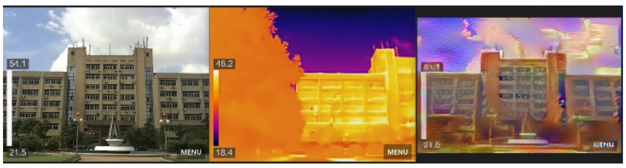

Fig. 6. Comparison of colored infrared style transfer for Algorithm II

Fig. 7. Comparison of black-and-white infrared style transfer for Algorithm II

In the two sets of results in Figs. 6 and 7, the generated effect images effectively retained the content features with a small loss of content details and preserved the texture features of the style images to certain extent. The distribution of style features is also highly uniform without distortion. Especially in the transferred images of the black-and-white infrared style images, the infrared style features are evident. However, the extraction of the color style features must be strengthened. The algorithm is generally consistent with the infrared effect observed by the human eye.

3.2.3 Algorithm II

Algorithm III also uses the VGG19 model to extract features but differs from the previous two algorithms in the selection of the feature extraction layer of the network model. Algorithm III extracts content features using conv5_2 of the VGG network and style features using conv1_1, conv2_1, conv3_1, conv4_1, and conv5_1 of the VGG network, discarding the fully connected layer. The ratio of content to style weights is 1,000,000:1. Figs. 8 and 9 show example transfer results for Algorithm III.

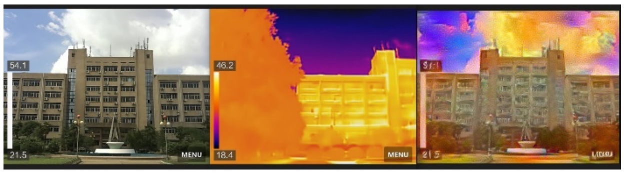

Fig. 8. Comparison of colored infrared style transfer for Algorithm III

Fig. 9. Comparison of black-and-white infrared style transfer for Algorithm III

Figs. 8 and 9 show that both sets of images remarkably well preserved the content characteristics of the content images, the content details remained intact, and the style characteristics are evident. However, a minimal difference lies in the style of color, and the overall performance is of the best among the three algorithms.

3.3 Evaluation of simulation results

A brief description of the image evaluation indexes for the evaluation of the simulation results is as follows: histogram, structural similarity (SSIM), and peak signal-to-noise ratio (PSNR). The effect maps are evaluated and compared with the real infrared style images of the same scene to analyze transfer effects of the images under different variables such as color and algorithm. (Note: For the evaluation of color variables, the test objects are the 25 colored and black-and-white infrared photo pairs; for the evaluation of algorithms, the test objects are the 10 colored and black-and-white infrared photo pairs each.)

3.3.1 Histogram

The histogram is considerably simpler compared to other evaluation metrics and can only capture the color information of the images. The two images are similar as long as the color distribution is the same between the effect and real maps.

3.3.2 SSIM

SSIM, also known as structural similarity, is a metric used to measure the similarity between real and effect maps. SSIM defines structural information as an attribute independent of brightness, contrast, and structure from the perspective of image composition, which is consistent with the judgment of the human eye in the measurement of image quality and belongs to subjective evaluation [27]. The value range of SSIM is [0,1]; a large SSIM value indicates a small image distortion.

The SSIM formula is based on three comparative measures between samples x (real maps) and y (effect maps): brightness, contrast, and structure. Equation (1) uses the mean value as an estimate of brightness, Equation (2) uses the standard deviation as an estimate of contrast, and Equation (3) uses the covariance as a measure of structural similarity [27].

$$l(x,y)=\frac{2\mu_x\mu_y+C_1}{\mu_x^2+\mu_y^2+C_1} \tag{1}$$

$$C(x,y)=\frac{2\sigma_x\sigma_y+C_2}{\sigma_x^2+\sigma_y^2+C_2} \tag{2}$$

$$s(x,y)=\frac{\sigma_{xy}+C_3}{\sigma_x\sigma_y+C_3} \tag{3}$$

Among them $C_1=(0.01*MAX_x)^2$; $C_2=(0.03*MAX_x)^2$; $C_3=\frac{C_2}{2}$; $MAX_x=255$. μ_x, μ_y are the mean values of samples x and y, respectively. σ_x^2, σ_y^2 are the variances of samples x and y, respectively. σ_{xy} is the covariance of x and y [27].

$$SSIM(x,y)=\left[l(x,y)^\alpha\cdot c(x,y)^\beta\cdot s(x,y)^\gamma\right] \tag{4}$$

Equation (4) represents the product of the percentage of three feature attributes (i.e., structural similarity). In this equation, α, β, and γ represent the proportion of different features in the SSIM measure, and $\alpha=\beta=\gamma=1$ is generally set in the actual calculation. Equations (1), (2), and (3) are substituted into Equation (4) and then simplified to obtain Equation (5).

$$SSIM(x,y)=\frac{(2\mu_x\mu_y+C_1)(2\sigma_{xy}+C_2)}{(\mu_x^2+\mu_y^2+C_1)(\sigma_x^2+\sigma_y^2+C_2)} \tag{5}$$

3.3.3 PSNR

PSNR is the abbreviation of "peak signal-to-noise ratio," which is an objective standard for evaluating images. PSNR is the most common and widely used objective measurement method for evaluating picture quality, but its scores cannot be fully consistent with the visual quality observed by the human eye [28]. Notably, the size of the two compared images must be the same. A large PSNR value leads to minimal distortion, and its mathematical formula is presented in Equation (6).

$$PSNR=10\times\log_{10}\left[\frac{(2^n-1)^2}{MSE}\right] \tag{6}$$

where n is the number of bits per sampled value, mean square error (MSE) is the square of the difference between the true and predicted values. The sum is then averaged [28].

$$MSE=\frac{1}{n}\sum_{i=1}^{n}\left(Y_i-\hat{Y}_i\right)^2 \tag{7}$$

Equation (7) is a representation of the MSE, where n denotes the total number of samples, Y_i denotes the true value, i.e., the real style map of the same scene; $\hat{Y}_i$ denotes the predicted value, i.e., the effect map.

4. Result Analysis and Discussion

Based on the image evaluation method in 3.3, the section evaluates the quality of the effect maps by the three image style transfer algorithms. First, the algorithm is set as a variable, other conditions are kept constant, and the transfer effects of the three algorithms are compared. The experimental data settings for the algorithmic variables are as follows: the first 10 photo pairs are colored infrared style image pairs, and the last 10 photo pairs are the black-and-white infrared style image pairs, revealing a total of 20 photo pairs. Second, the color of the infrared image is set as a variable while keeping other conditions unchanged. The experimental data settings for the color variables are as follows: 25 groups each of colored infrared style image pairs and black-and-white infrared style image pairs.

4.1 Histogram evaluation results

The transfer effects of the three different algorithms are compared and analyzed using histogram evaluation metrics, and the results are shown in Fig. 10. The figure reveals that Algorithm III generally has the best and most stable transfer results, indicating that Algorithm III outperforms the two other algorithms in the extraction of style color features. Algorithm I preserves certain stylistic features. However, the distribution of stylistic features is uneven and appears distorted, and the color distribution of the real style map markedly differs, yielding low histogram evaluation results. The color distribution of the resultant images of Algorithm II is even, but the color features are not sufficiently distinct, which leads to low histogram values.

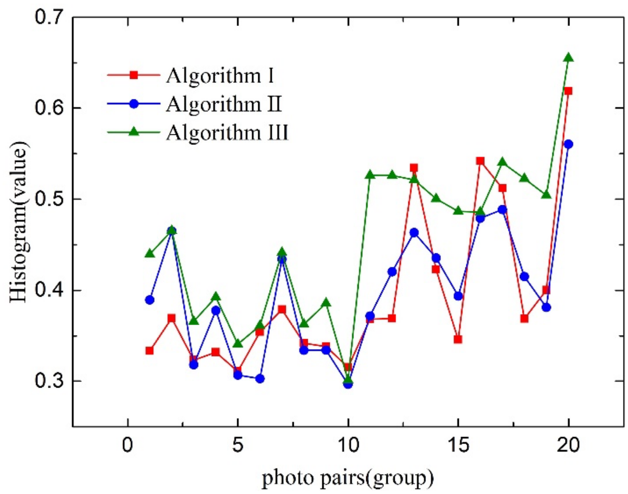

Fig. 10. Comparison of histogram evaluation of the three algorithms

The color of the style images is then set as the variable, and the histogram evaluation of the effect maps generated under different colored infrared style images of the same algorithm is compared to analyze the impact of colors of style images on the transfer results. The results are shown in Figs. 11, 12, and 13. The histogram evaluation results by the transferring method of the black-and-white style images are the best in all three algorithms. The black-and-white infrared style images have single color and are convenient in style feature extraction; thus, the color distribution is uniform in the style transfer process, and the style features of the style images are effectively retained. Moreover, histogram evaluation mainly captures the color information of the images. Therefore, the evaluation results of the effect map generated under black-and-white infrared style images are superior. Fig. 11 shows that the effect maps of transferring in colored infrared style images are more stable than those in black-and-white infrared style, indicating that Algorithm I is suitable for the transfer of colored infrared style images.

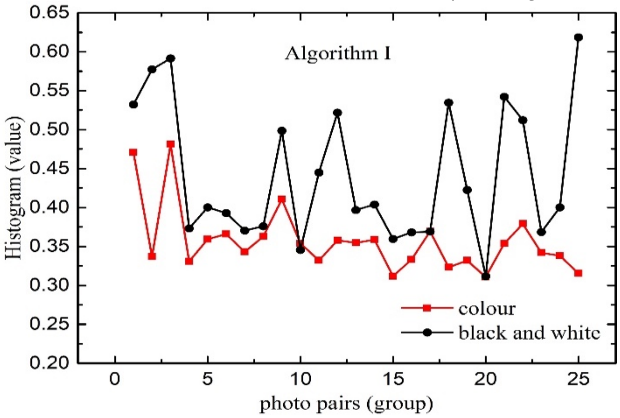

Fig. 11. Comparison of histogram evaluation for Algorithm I

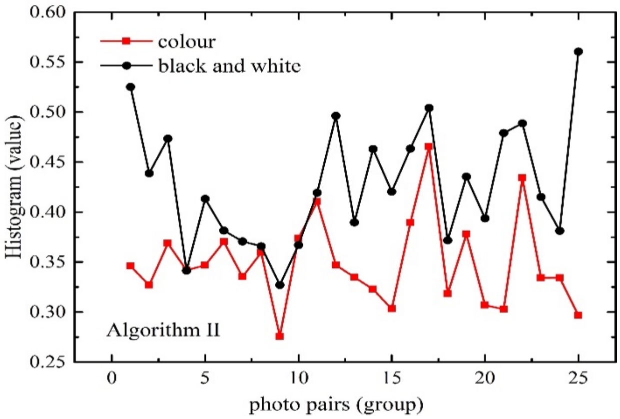

Fig. 12. Comparison of histogram evaluation for Algorithm II

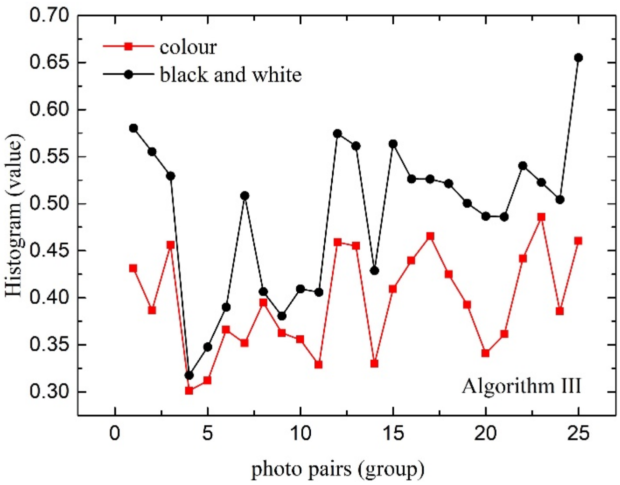

Fig. 13. Comparison of histogram evaluation for Algorithm III

4.2 SSIM evaluation results

First, the SSIM of the transfer effect maps of the three algorithms are compared, and the results are shown in Fig. 14. The SSIM values for the first 10 color infrared style image pairs of the three algorithms are significantly lower than those of the last 10 black-and-white infrared style image pairs. The results of Algorithm II perform best overall, which is in line with the judgment of human eye.

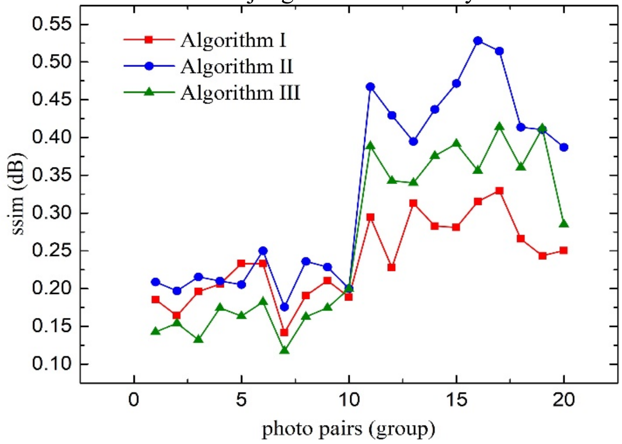

Fig. 14. Comparison of SSIM evaluation of three algorithms

The colors of the style images are then set as the variables to evaluate the quality of the effect maps transferred from the three algorithms using structural similarity. The evaluation results are shown in Figs. 15, 16, and 17. The values of the maps generated under black-and-white infrared style images are high, but a few individual samples with different performances. However, in all three algorithms, the results of colored infrared style images are more stable than those of black-and-white infrared style images.

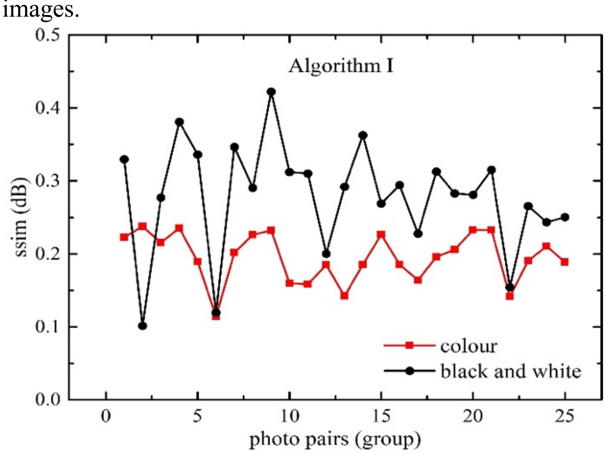

Fig. 15. Comparison of SSIM evaluation for Algorithm I

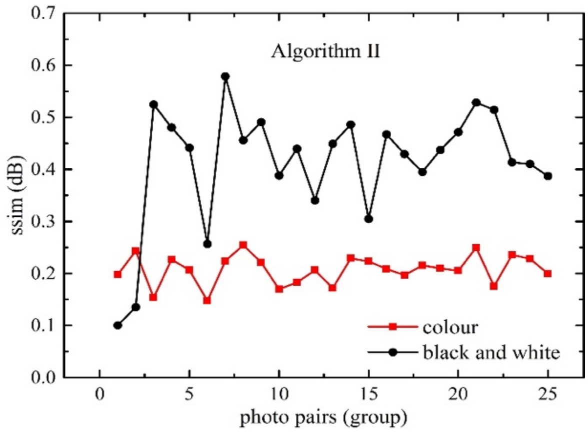

Fig. 16. Comparison of SSIM evaluation for Algorithm II

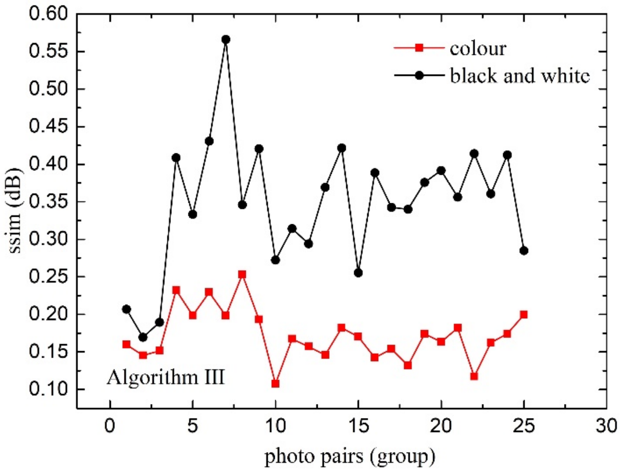

Fig. 17. Comparison of SSIM evaluation for Algorithm III

4.3 PSNR evaluation results

Fig. 18 shows a comparison of the PSNR evaluations of the three algorithms. The figure reveals that in the PSNR evaluation of the first 10 colored infrared style image pairs, the quality of the results of Algorithm I is higher than that of the two other algorithms, while the evaluation data quality of the two algorithms is identical. The infrared style photos do not stand out in content details. Thus, highlighting the characteristics of the infrared style without excessive retention of content details is rather better for Algorithm I, allowing this algorithm to produce the transfer effect maps that conform to the infrared image style in the objective evaluation. By contrast, Algorithm III performs best for the quality assessment of the last 10 photo pairs of black-and-white infrared style images.

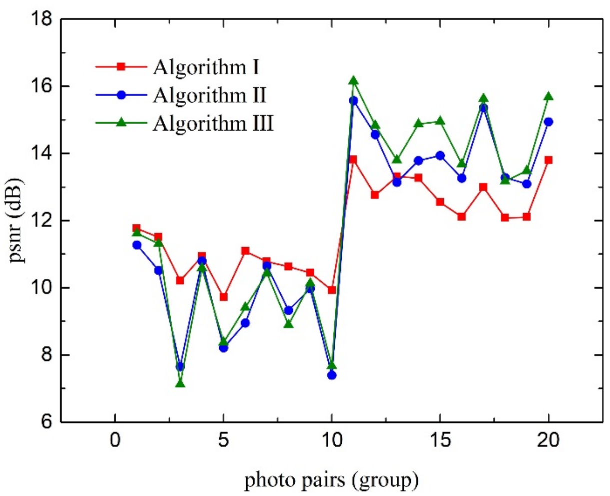

Fig. 18. Comparison of PSNR evaluation of three algorithms

Figs. 19, 20, and 21 represent the PSNR evaluation of the three algorithms under different color style images. Similarly, the transfer effect in all three algorithms is superior under the black-and-white infrared style images. The style color features of black-and-white infrared style images are monotonous. Thus, the style features extracted from the network layer are complete, allowing the three algorithms to retain the style features better with less distortion compared to the colored infrared style. Therefore, the transfer effect of black-and-white infrared style images is superior.

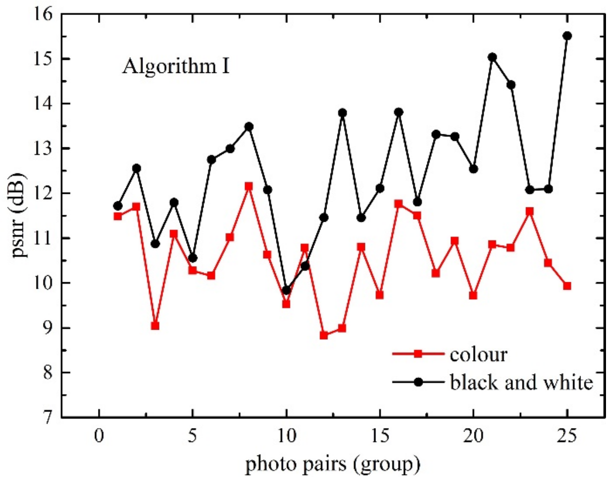

Fig. 19. Comparison of PSNR evaluation for Algorithm I

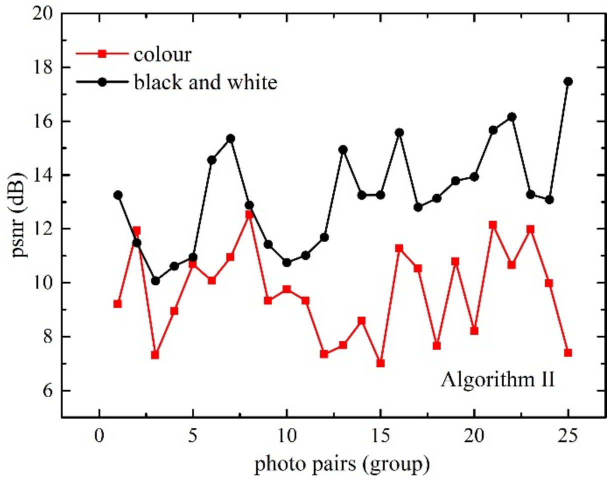

Fig. 20. Comparison of PSNR evaluation for Algorithm II

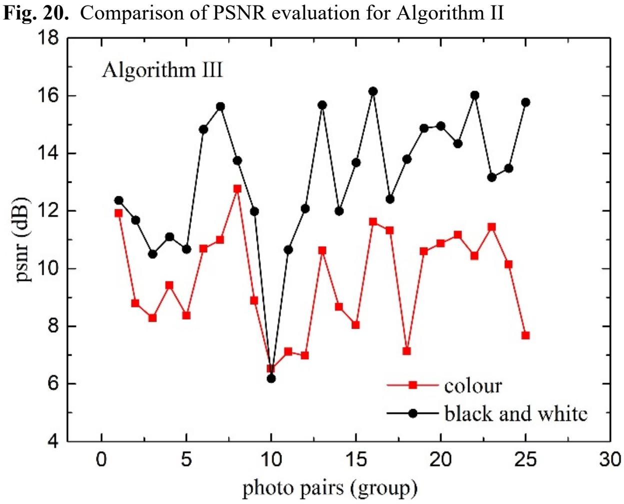

Fig. 21. Comparison of PSNR evaluation for Algorithm III

4.4 Analysis

Fig. 4 shows the transfer effect of Algorithm I. The content feature extraction layers in Algorithm I comprise five convolution layers, which retains the high-dimensional feature information of the content image and low-dimensional feature information such as texture and color, resulting in extraction distortion of content features and poor visual effects in the simulated effect images. Fig. 6 shows the transfer effect of Algorithm II, which has a good overall visual effect with a small amount of loss of content details. Algorithm II selected Conv5_2 and Conv4_2 deep convolution layers as the content extraction layers, only extracting high-dimensional feature information such as the shape of the content images. Therefore, the content features show good performance, but the style features must still be strengthened. Fig. 8 shows the transfer effect of Algorithm III, where the transfer effect is better compared to that of Figs. 4 and 6. The content feature extraction layer of Algorithm III is a deep convolution layer Conv5_2, the retention of content features is more complete compared to Algorithm II, and no loss is observed. Thus, the selection of the feature extraction convolution layer affects the generation of infrared images.

The data from the algorithm evaluation comparisons in Figs. 10, 14, and 18 are averaged and plotted in Table 1 below, where Algorithm III has the highest histogram and PSNR evaluation indexes, and Algorithm II has the highest SSIM values. All the quality evaluation charts in Chapter 4 reveal a few individually large gaps in the evaluation results between images because the experimentally selected simulation data pairs have different scene categories, resulting in large gaps in the content complexity and colors between the images. For the real infrared images, the content details of the images are not observed, while the algorithm retains additional content features. Therefore, the simulated effect maps have the detail features of the content that the real infrared images do not have, hence the image quality assessment results are lower. In addition, some angle deviations exist when shooting image data manually, which leads to differences in the evaluation and comparison of the content or structure of the images.

Table. 1. Mean values of each evaluation indicator for the three algorithms

	Algorithm I	**Algorithm II**	**Algorithm III**
Histogram	0.3940	0.3986	0.4564
SSIM (dB)	0.2375	0.3290	0.2634
PSNR (dB)	11.7888	11.7855	12.0927

5. Conclusions

This study adopted a total of three GAN-based image style transfer algorithms to implement infrared view simulation and evaluated the simulation results of the three algorithms to explore the method of infrared texture generation and reveal the impact of GAN. Finally, the following conclusions could be drawn:

(1) This experiment uses real-life visible infrared images to conduction simulations to verify the effectiveness of the GAN-based image style transfer method for infrared texture generation. The visible light images can be converted into images with infrared texture styles without training data.

(2) The simulation results of the three algorithms show that the transfer effect of black-and-white infrared style images is better than those of the colored infrared style images.

(3) The evaluation results reveal that selecting the deep convolution layer in the VGG network as the content feature extraction layer is favorable for the generation of the infrared texture.

This study combines indoor simulation experiments with theoretical research, proposes a new direction of infrared texture generation for infrared view simulation technology, and constructed network models of infrared style transfer algorithm that can realize the conversion of visible light to infrared images, which is of important reference significance for the subsequent research of infrared view simulation. Therefore, the infrared image style transfer algorithm will be optimized in future research, making the simulation generated by the effect maps are close to the real infrared images.

Acknowledgements
This work was supported by the National Nature Science Fund of China (81801784), the Natural Science Foundation of Education Department of Hubei Province (B2020149, Q20162706), and the Natural Science Foundation of Xiaogan City (XGKJ2022010095).

References

[1] X. Wang, H. Wang, C. Xu, Y. Z. Bai, and W. Q. Jin, "Overview on development of infrared scene simulation," *Infrared Technol*., vol. 37, no. 7, pp. 537-543, Jul. 2015.

[2] Y. Shen, C. H. Huang, F. Huang, J. Li, and M. J. Zhu, "Research progress of infrared and visible image fusion technology," *Infrared Laser Eng.*, vol. 50, no. 9, 2021, Art. no. 20200467, doi: 10.3788/IRLA20200467.

[3] A. Patel and J. Chaudhary, "A review on infrared and visible image fusion techniques," in *Intell. Commun. Technol. Virtual Mob. Netw., ICICV 2019*., Tirunelveli, India, 2020, pp. 127-144.

[4] G. Y. Chen, X. J. Wu, and T. Y. Xu, "Unsupervised fusion algorithm for infrared and visible images based on deep learning," *J. Optoelect. Laser*, vol. 59, no. 04, pp. 151-160, Feb. 2022.

[5] W. Ma, *et al*, "Infrared and visible image fusion technology and application: a review," *Sensors*, vol. 23, no. 2, pp. 599, Jan. 2023.

[6] J. Latger, T. Cathala, N. Douchin, and A. L. Goff, "Simulation of active and passive infrared images using the SE-WORKBENCH," in *Proc. SPIE-Infrared Imag. Syst., Des., Anal., Model., Test. XVIII*, Orlando, FL, USA, 2007, pp. 11-25.

[7] J. F. Lepage, M. A. Labrie, and E. Rouleau, "DRDC's approach to IR scene generation for IRCM simulation," in *Proc. SPIE-Technol. Synth. Environ., Hardw. Loop XVI*, Orlando, FL, USA, 2011, pp. 143-152.

[8] R. Guissin, *et al*, "IRISIM: infrared imaging simulator," in *Proc. SPIE-Infrared Imag. Syst., Des., Anal., Model., Test. XVI*, Orlando, FL, USA, 2005, pp. 190-200.

[9] L. Swierkowski, C. L. Christie, L. Antanovskii, and E. Gouthas, "Real-time scene and signature generation for ladar and imaging sensors," in *Proc. SPIE-Infrared Imag. Syst., Des., Anal., Model., Test. XXV*, Baltimore, MD, USA, 2014, pp. 462-475.

[10] U. Sakoglu and M. C. Minton, "Development of an algebraic nonuniformity correction algorithm for hexagonally-sampled infrared imagery," in *Proc. SPIE-Infrared Sens. Dev. Appl. X*, 2020, pp. 27-37. [Online]. Available: https://www.spie.org/Publications/Proceedings/Volume/11503#_=_

[11] M. Ogata, S. Murakami, and T. Mikura. (2020). Privacy-preserving monitoring system with ultra low-resolution infrared sensors. Presented at 2th Workshop Artif. Intell. Func., Disabil., Health. [Online]. Available: https://ai4function.github.io/2021/

[12]M. Duris, D. Deubel, L. Bodiou, C. Vaudry, J. C. Keromnes, and J. Charrier, "Fabrication of Ge-ZnS multilayered optical filters for mid-infrared applications," *Thin Solid Films*, vol. 719, Feb. 2021, Art. no.138488.

[13]I. Mal, S. Singh, and D. P. Samajdar, "Design and simulation of InAsBi PIN photodetector for long wavelength infrared applications," *Mater. Today: Proc*., vol. 57, Part 1, pp. 289-294, Feb. 2022.

[14] P. D. Klaassen, *et al*, “MIRISIM: a simulator for the Mid-Infrared Instrument on JWST,” *Mon. Not. R. Astron*, *Soc.*, vol. 500, no. 3, pp. 2813-2821, Jan. 2021.
[15] X. P. Shao, “Research on infrared texture generation method,” Ph.D. dissertation, Dept. Optical Eng., Xidian Univ., Xi’an, China, 2005.
[16] C. Zhao, “Research on OGRE-oriented infrared texture design and generation method,” M.S. thesis, Dept. Phi., Xidian Univ., Xi’an, China, 2010.
[17] L. H. Gao, “Generation of ground background infrared texture and its application in scene simulation,” M.S. thesis, Dept. Phi., Xidian Univ., Xi’an, China, 2013.
[18] Y. M. Jiang, “Design of infrared real-time simulation system for optoelectronic interference coupling scenario,” M.S. thesis, Dept. Control Sci. Eng., Huazhong Univ. Sci. Technol., Wuhan, China, 2019.
[19] Y. Zhang, Y. Gao, Y. Y. Ma, and H. Y. Qu, “Overview of a new type of large dynamic infrared imaging simulation technology,” in *Chin. Simul. Conf. 2020*, Beijing, China, 2020, pp. 118-123.
[20] C. Y. Li, L. G. Li, Z. Yang, and W. Ni, “Infrared imaging simulation framework and implementation based on 3D scene,” *Comput. Simul.*, vol. 37, no. 07, pp. 248-252, Jul. 2020.
[21] Y. F. Liu, “Design and implementation of real-time infrared images simulation engine based on OpenGL,” M.S. thesis, Dept. Detect. Technol. Autom. Equip., Xidian Univ., Xi’an, China, 2021.
[22] L. M. Zhao, L. S. Zhong, and X. S. Ge, “Design of an airborne infrared jamming shell simulation system based on Unity3D visual scene,” *Electron. Inf. Warf. Technol*., vol. 37, no. 06, pp. 66-71, Nov. 2022.
[23] L. A. Gatys, A. S. Ecker, and M. Bethge, “Texture synthesis using convolutional neural networks,” in *Neural Inf. Process. Syst.,* Montreal, Canada, 2015, pp. 262-270.
[24] L. A. Gatys, A. S. Ecker, and M. Bethge, “Image style transfer using convolutional neural networks,” in *Proc. IEEE Conf. Comput. Vis. Pattern Recog.*, Las Vegas, NV, USA, 2016, pp. 2414-2423.
[25] Q. Z. Mou, Q. Zhou, X. N. Song, and C. P. Sun, “Research on fast generation of infrared images of large-scale ground scenes based on feature transfer network,” *Intell. Comput. Appl.*, vol. 13, no. 09, pp. 184-188+193, Sept. 2023.
[26] S. Mascarenhas and M. Agarwal, “A comparison between VGG16, VGG19 and ResNet50 architecture frameworks for image classification,” in *Proc. 2021 Int. Conf. Disrupt. Technol. Multi-discip. Res. Appl*., Bengaluru, India, 2021, pp. 96-99.
[27] A. Hore and D. Ziou, “Image Quality Metrics: PSNR vs SSIM,” in *Proc. 20th Int. Conf. Pattern Recog*., Istanbul, Turkey, 2010, pp. 2366-2369.
[28] U. Sara, M. Akter, and M. S. Uddin, “Image quality assessment through FSIM, SSIM, MSE and PSNR—a comparative study,” *J. Comput. Commun*., vol. 7, no. 3, pp. 8-18, Mar. 2019.